THE END OF THE MACHO ERA, REVISITED: NEW LIMITS ON MACHO MASSES FROM HALO WIDE BINARIES

Miguel A. Monroy-Rodríguez and Christine Allen

Instituto de Astronomía, Universidad Nacional Autónoma de México, Apdo. Postal 70-264, México,
D.F. 04510, Mexico; chris@astro.unam.mx

ABSTRACT

In order to determine an upper bound for the mass of the massive compact halo objects (MACHOs), we use the halo binaries contained in a recent catalog by Allen & Monroy-Rodríguez. To dynamically model their interactions with massive perturbers, a Monte Carlo simulation is conducted, using an impulsive approximation method and assuming a galactic halo constituted by massive particles of a characteristic mass. The results of such simulations are compared with several subsamples of our improved catalog of candidate halo wide binaries. In accordance with Quinn et al., we also find our results to be very sensitive to the widest binaries. However, our larger sample, together with the fact that we can obtain galactic orbits for 150 of our systems, allows a more reliable estimate of the maximum MACHO mass than that obtained previously. If we employ the entire sample of 211 candidate halo stars we, obtain an upper limit of $112\,M_\odot$. However, using the 150 binaries in our catalog with computed galactic orbits, we are able to refine our fitting criteria. Thus, for the 100 most halo-like binaries we obtain a maximum MACHO mass of 21–$68\,M_\odot$. Furthermore, we can estimate the dynamical effects of the galactic disk using binary samples that spend progressively shorter times within the disk. By extrapolating the limits obtained for our most reliable—albeit smallest—sample, we find that as the time spent within the disk tends to zero, the upper bound of the MACHO mass tends to less than $5\,M_\odot$. The non-uniform density of the halo has also been taken into account, but the limit obtained, less than $5\,M_\odot$, does not differ much from the previous one. Together with microlensing studies that provide lower limits on the MACHO mass, our results essentially exclude the existence of such objects in the galactic halo.

Key words: binaries: general – dark matter – Galaxy: halo – stars: kinematics and dynamics – stars: statistics

1. INTRODUCTION

Disk and halo binaries are relevant to the understanding of the processes of star formation and early dynamical evolution. In particular, the orbital properties of the wide binaries remain unchanged after their formation, except for the effects of their interaction with perturbing masses encountered during their lifetimes as they travel in the galactic environment. The widest binaries are quite fragile and easily disrupted by encounters with various perturbers, be they stars, molecular clouds, spiral arms, or massive compact halo objects (MACHOs). For this reason, they can be used as probes to establish the properties of such perturbers. The use of wide binaries as sensors of the dynamical effects of perturbers in the galactic halo has been the subject of several studies (Yoo et al. 2004, Quinn et al. 2009). An interesting application of halo wide binaries was proposed by Yoo et al. (2004) who used 90 halo binaries from the catalog of Chanamé & Gould (2004, hereinafter ChG) to try to detect the signature of disruptive effects of MACHOs in their widest binaries. They were able to constrain the masses of such perturbers to $M < 43\,M_\odot$, practically excluding MACHOs from the galactic halo since other studies (Alfonso et al. 2003; Tisserand et al. 2007; Wyrzykowski et al. 2009, 2011) exclude objects with masses in the range of $10^{-7}\,M_\odot < M < 15\,M_\odot$. However, as was shown a few years later by Quinn et al. (2009) this result depends critically on the widest binaries of their sample as well as on the observed distribution of the angular separations which, according to ChG, shows no discernible cutoff between $3\farcs5$ and $900''$. Quinn et al. (2009) obtained radial velocities for both components of four of the widest binaries in the ChG catalog and found concordant values for three of them, thus establishing their physical nature. The fourth

binary turned out to be optical, resulting from the random association of two unrelated stars. Quinn et al. excluded this spurious pair from their study. They assumed a power-law distribution for the initial projected binary separation and varied the exponent over a wide range. They evolved the distributions and compared their results with the distribution of the observed projected separations, attempting a best fit of the models to the observed distribution. Quinn et al. found a limit for the masses of the MACHOs of $M < 500\,M_\odot$, much less stringent than that previously obtained. They concluded rather pessimistically that the currently available wide binary sample is too small to place meaningful constraints on the MACHO masses. They also pointed out that the density of perturbers encountered by the binaries along their galactic orbits is variable, and that this variation should be taken into account when calculating constraints on MACHO masses.

Motivated by these concerns, we have constructed a catalog of 211 candidate halo wide binaries (Allen & Monroy-Rodríguez 2014) and computed galactic orbits for 150 such binaries. The orbits allowed us to establish the fraction of its lifetime each binary spends within the galactic disk and thus to estimate the dynamical effects of the passage of the binary through the disk. The orbits also allow us to estimate the effects of the variable halo density encountered by the binaries along their galactic trajectories. We stress that for a total of nine of the widest binaries, concordant radial velocities for both components were found in the literature, thus confirming their physical association. The radial velocities of both components of these pairs were found to be equal within the published observational uncertainties. A more sophisticated analysis was not attempted because the random association of two unrelated stars will most probably result in grossly discrepant radial

velocities. Inspection of Table 1 in Quinn et al. (2009) shows that, indeed, the radial velocities of their three physical pairs are equal within the stated uncertainties, whereas the components of the non-physical pair have radial velocities differing by almost 80 km s^{-1}.

2. THE DYNAMICAL MODEL

To model the dynamical evolution of our sample of halo wide binaries, we follow closely the procedure of Yoo et al. (2004). In this approach, the impulse approximation is used, and effects of large-scale galactic tides and molecular clouds are neglected. Yoo et al. (2004) give a detailed description of the impulse approximation. Dissolved binaries are eliminated from the modeled population. The galactic mass distribution is assumed to be constant over time. Thus, the effects of major mergers are ignored. Such mergers would possibly be quite destructive for fragile systems such as wide binaries. On the other hand, they could also be a source of fresh wide binaries acquired by our Galaxy (Allen et al. 2007). The dynamical and merger history of our galaxy is at present too poorly known to take into account in our model.

We initially assume a constant halo density and attribute to the MACHOs the total local halo density, taken as $\rho = 0.007\,M_\odot\,{\rm pc}^{-3}$. This value is taken from the Allen & Santillán (1991) mass model for consistency with the computed galactic orbits of the wide binaries. It is quite similar to the values used by Yoo et al. (2004) and Quinn et al. (2009). It also agrees with the value obtained by Widrow et al. (2008). We then evaluate the effects of the 100 closest encounters in the tidal regime and compute the cumulative effects of weak encounters in the Coulomb regime.

We start the Monte Carlo simulations by drawing initial semiaxes uniformly from a power-law distribution with an arbitrary exponent and with separations between 10 AU and 300,000 AU The mass of each binary component is taken as $0.5\,M_\odot$, and the velocity distribution of the perturbers is assumed to be isotropic with a dispersion of 200 km s^{-1} in each component, appropriate for halo objects. In each model simulation, we let 100,000 binary systems evolve for 10 Gy. For each model (with a fixed MACHO mass M and a fixed local halo density), we construct a scattering matrix to simultaneously investigate large sets of initial power-law distributions. This scattering matrix gives the probability that a binary with initial semiaxis a will have a semiaxis a' after 10 Gyr of evolution. For each model we generate a virtual binary sample with the same number of binaries as the observed sample such that the number of binaries with major semiaxes between $a_{\rm min}$ and $a_{\rm max}$ is equal to the observed number of binaries within these limits. These limits will be different for the different subsamples used to estimate the maximum MACHO mass. The virtual binary samples resulting from the evolved model are then compared with the observed samples of binaries. For comparison with the binned observational data, each bin of virtual binaries is taken as the centroid of the corresponding group of model binaries, comprising about 10,000 binaries. For comparison with the unbinned observational data each virtual binary is constructed as the centroid of more than 500 evolved binaries (for the comparison with the 100 most halo-like binaries), and of more than 2600 (for comparing with the 25 most halo-like binaries). In all cases, therefore, each virtual binary represents a sufficiently large number of evolved model binaries, and hence sampling errors are negligible.

The goodness of fit is evaluated by minimizing the dispersion, σ, defined as

$$\sigma = \frac{\sqrt{\sum_i \left(\langle a \rangle_{\rm obs} - \langle a \rangle_{\rm virtual}\right)^2}}{N},$$

where $\langle a \rangle_{\rm obs}$, $\langle a \rangle_{\rm virtual}$ are the expected major semiaxes of the observed and the virtual binary, respectively, and N is the number of binaries in the sample. For the purpose of comparing our results with previous ones, we also computed the σ from a maximum likelihood estimate, adhering to the definition of σ used by Quinn et al. (2009). We stress that the distributions of semiaxes of the simulated and the observed binary samples are compared directly. Previous work (Yoo & Chaname; Quinn et al. 2009) fitted the observed projected separations. Since distances are available for all our binaries, we prefer to compare directly the resulting model distribution of major semiaxes with the observed one, calculated from the angular separations and the individual distances. Projection effects are taken into account by means of the widely used statistical formula (Couteau 1960):

$$\langle a'' \rangle = 1.40 s''.$$

This formula was derived theoretically and includes the eccentricity distribution of the binaries, as well as projection effects. Here, $\langle a \rangle$ represents the expected value of the major semiaxis a and s the angular separation. A more recent empirical study (Bartkevičius 2008) compares the angular separations with the major semiaxes for systems from the Catalog of Orbits of Visual Binaries (Hartkopf & Mason 2007). The results obtained vary somewhat according to the data used for the separations s, either from "first" or "last" observations in the WDS (Mason et al. 2001), or from the orbit catalog ephemerides, the latter deemed to provide the most reliable value, namely,

$$\log \langle a \rangle - \log s = 0.112.$$

In spite of the rather large uncertainties of the latter values, we shall use both estimates to compute the maximum MACHO masses.

The individual distances to the binaries used to convert separations in arcsec into separations in AU and then into expected major semiaxes have, of course, observational uncertainties. Since the groups of binaries we will use to determine maximum MACHO masses contain binaries from different sources, we can only provide an estimated average uncertainty for the distances, as we are trying to err on the conservative side. In our catalog, we adopted the distances given in the *Hipparcos* catalog when their parallax errors were less than 15%. Otherwise, we adopted, in order of preference, the Strömgren photometric distances given in the lists of Nissen & Schuster (1991); those obtained with the polynomial of ChG, using their photometry; or the spectroscopically derived distances of Ryan (1992) and Zapatero-Osorio & Marttín (2004). Most of our binaries should have distance errors of less than about 15%.

To obtain the values of the power-law exponent and the maximum MACHO mass compatible with the observations, we proceed as follows. We start by assuming the mass of the perturbers to be zero and multiply the scattering matrix by power laws, letting the exponent vary between -1 and -2 (in increments of 0.01), until the best fit of the virtual binary sample to the observed distribution is found; by "best fit" we mean the fit that minimizes the dispersion σ as defined above. This fit is characterized by a dispersion $\sigma = \sigma_0$. Then we repeat
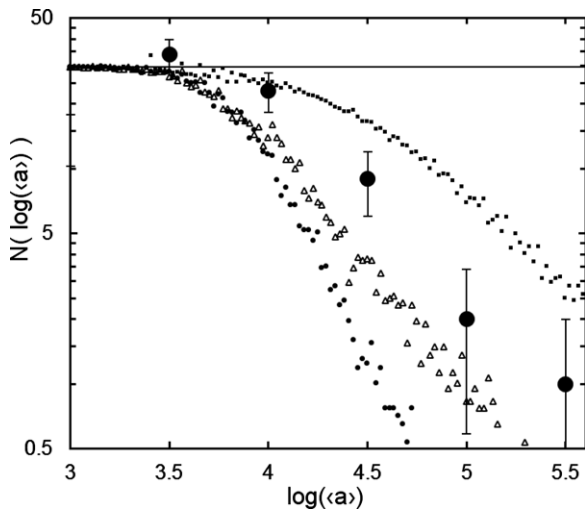
Figure 1. Evolved distribution of semiaxes for various perurber masses. The model was applied to the Quinn et al. (2009) binaries. Dots correspond to perturber masses of 1000 $M_\odot$, triangles to 100 $M_\odot$, and small squares to 10 $M_\odot$. Each symbol represents 500 modeled binaries. The graph shows results very similar to those of Yoo et al. (2004) and Quinn et al. Perturber masses of 1000 $M_\odot$ appear to be too large, while masses below 10 $M_\odot$ seem too small to reproduce the observed distribution (large dots). The bars in the observed distribution correspond to sampling errors.

Figure 2. Exclusion contour plot. The thick gray lines denote the limits from microlensing experiments and galactic disk stability. The thin dashed line is the result of Yoo et al. (2004) for 90 binaries. The thick dashed line is our result for the same sample using their method. Both results agree reasonably well. The thin solid line is the result of Quinn et al. (2009) for the 90 original Yoo et al. binaries. The thick solid line is our result for the same sample, using a fit to 2σ. Here again, the results agree well. Finally, the thick dotted line refers to the result of Quinn et al. for 89 binaries, omitting one spurious pair. The concordance of previous results with our method applied to the same samples of binaries appears satisfactory, especially in the region of large halo densities and small perturber masses, which is the interesting region. Previous work dealt with projected angular separations. We deal with semiaxes, and therefore the results cannot be expected to be identical.

the procedure, increasing the perturber mass in increments of $1\,M_\odot$ until a fit is obtained with $\sigma = 2\sigma_0$, which we take as still acceptable. This yields a more conservative estimate of the maximum MACHO mass but still compatible (within $2\sigma_0$) with the observations.
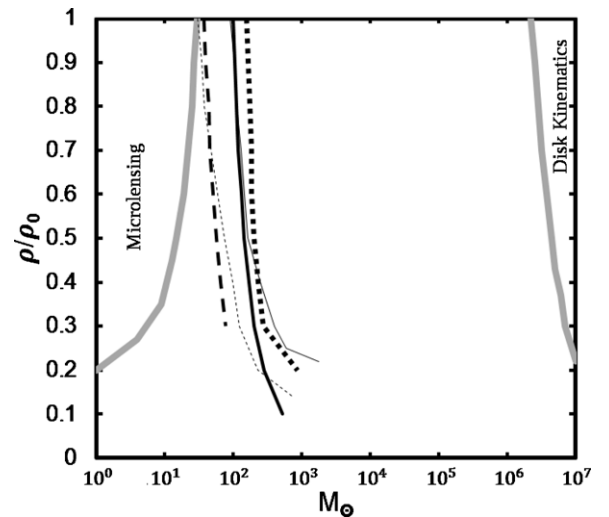
Our implementation of the dynamical model was tested by applying it to the binary samples studied by Yoo et al. (2004) and Quinn et al. (2009).

Figure 1 shows the results of applying our dynamical model to the binaries of Yoo et al. Qualitatively, it is seen that perturber masses of 1000 $M_\odot$ and 100 $M_\odot$ appear to be excessive, while perturber masses of 10 $M_\odot$ are insufficient to account for the observed distribution. This figure shows results very similar to those of previous studies (see, e.g., Figure 5 in Yoo et al.).

Figure 1 also shows that the horizontal line (exponent -1) represents the initial—unevolved—distribution which has to evolve farthest in order to fit the observed distribution, that is, that which needs the largest mass of perturbers to conform with observations. In this sense, taking an initial distribution with a -1 exponent yields the most conservative estimate for the perturber mass, i.e., the largest MACHO mass.

Figure 2 shows the exclusion contours we obtain by applying our model to the Yoo et al. and Quinn et al. samples. Since we are comparing semiaxes instead of projected angular separations, an exact match is not to be expected. Nonetheless, our results closely agree with previous ones, especially in the region of large halo densities and small perturber masses, which is the interesting one.

The range of exponents considered for the initial power-law distribution of our model binaries amply covers the observationally found ones. So, for example, ChG find -1.67 and -1.55 for their disk and halo binaries, respectively. Sesar et al. (2008) find -1; Lépine & Bongiorno (2007) obtain -1; Poveda et al. (1994, 1997), Poveda & Hernández-Alcántara (2003), and Poveda & Allen (2004) find -1 but up to different limiting semiaxes according to the age of the binaries; finally, Allen et al. (2000) find -1 for their high-velocity metal-poor binaries, but also only up

to different limiting semiaxes, according to the time spent by the binaries within the galactic disk.

Furthermore, as also pointed out by Quinn et al., there are both theoretical and observational reasons to justify the assumption of a -1 exponent for the unevolved distribution. Indeed, Valtonen (1997) showed Oepik's distribution to correspond to dynamical equilibrium, and it has been found to hold for many different samples of wide binaries of different ages and provenances (Poveda et al. 2007; Sesar et al. 2008; Lépine & Bongiorno 2007; Allen et al. 2000). In the accompanying paper (Allen & Monroy-Rodríguez 2014), we show that it holds for halo binaries up to different limiting semiaxes, according to the time the binaries spend within the galactic disk. For the most halo-like binaries, it holds up to expected semiaxes of 63,000 AU.

As pointed out by Quinn et al. the results are dependent on the definition of σ. We adhere to the definition of Quinn et al. to compare our results with theirs. However, we found that the maximum likelihood method does not give as good a resolution for the MACHO mass as that obtained using the ordinary dispersion σ as defined above or using the Kolmogorov–Smirnov (K-S) indicator for the unbinned distributions, as we describe below.

The best fit between the virtual binary distribution and the observed one fixes the value of M, the mass of the perturbers. As explained above, the most conservative estimate (largest MACHO mass) is obtained for an exponent of -1, which corresponds to the Oepik distribution.

As an illustration, Figure 3 shows the results of the numerical simulation compared to the observed groups of the 100, 50, and 25 most halo-like binaries from our catalog. The frequency distribution of expected semiaxes is plotted in the vertical axis. The large dots indicate the observed distribution, with error bars corresponding to sampling errors. The horizontal
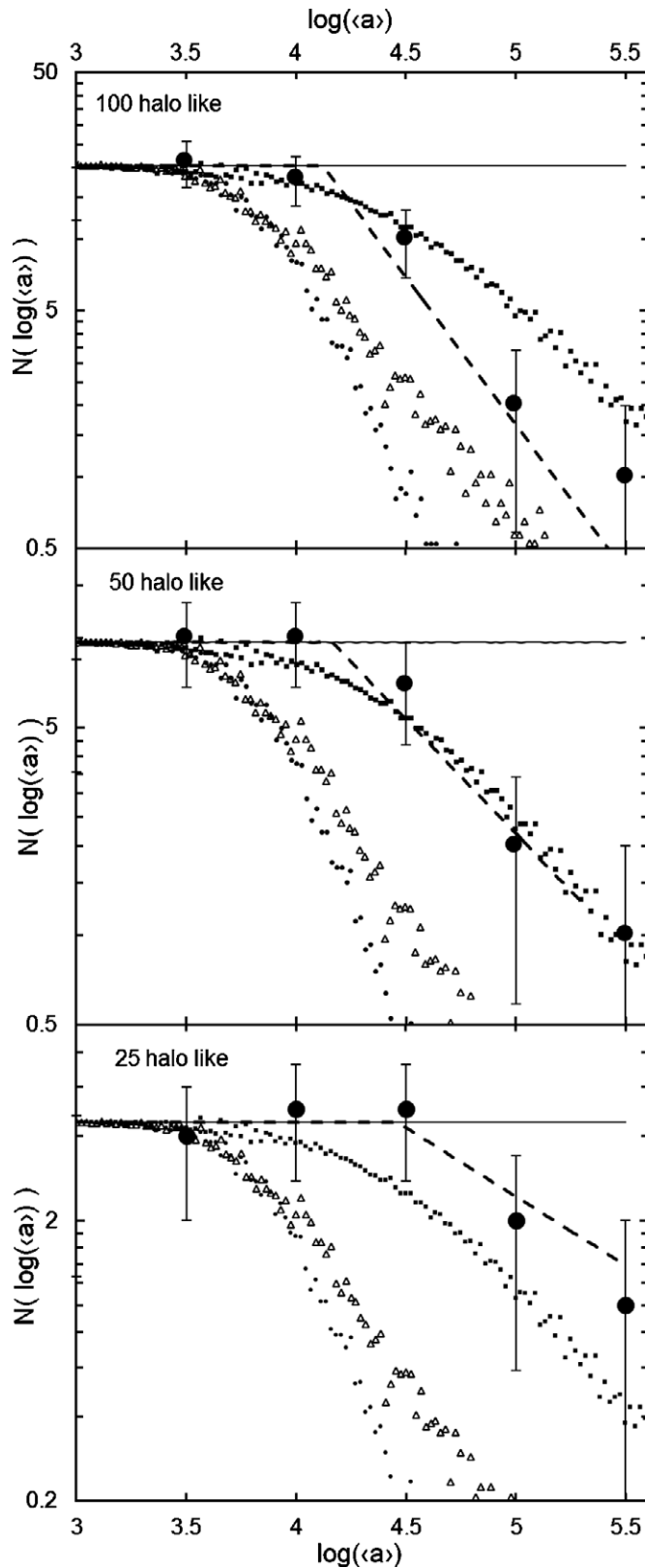
Figure 3. Evolved distribution of semiaxes for different perturber masses, compared with three samples of binaries from our catalog. The straight horizontal line shows the initial distribution. The large dots with error bars denote the observed data. The dashed lines show the two power-law fits to the observed samples, namely an Oepik law fit to the unevolved region and a steeper power law for the evolved region (see the text). Filled squares correspond to perturber masses of $10\,M_{\odot}$, triangles to $100\,M_{\odot}$, and dots to $1000\,M_{\odot}$. Depending on the sample considered, perturber masses of several hundreds $M_{\odot}$, about $10\,M_{\odot}$ and less than $10\,M_{\odot}$ appear to fit respectively the 100, 50, and 25 most halo-like binaries.

line corresponds to an unevolved binary population with a power-law exponent of -1. The dashed line shows the best fit we obtain for the observed distribution, using two power laws for the unperturbed and perturbed part, respectively (see below). The figure shows qualitatively how, depending on the observed sample, the admissible perturber masses range from about $50\,M_{\odot}$ to less than $10\,M_{\odot}$.

To construct Figure 3, we started by fitting each observed sample with a power law of exponent $\alpha = -1$ up to the value of the semiaxis where dissolution effects become noticeable. As shown in the companion paper (Allen & Monroy-Rodríguez 2014) the K-S test shows this fit to be valid up to different values of the semiaxes. We refer to this region as the unperturbed region. For the perturbed region (larger values of the semiaxes) we use a steeper power-law fit. The K-S test shows (see, e.g., Figure 5) that using two power-law fits allows an excellent representation of the observed samples for the entire range of semiaxes.

The virtual binary samples obtained from the evolved model binaries are then compared with these fits. Figure 4 shows an example of the comparison with the samples of the 100, 50, and 25 most halo-like stars. The large dots represent the observed sample. The full squares were obtained by varying the perturber mass in intervals of $1\,M_{\odot}$ until the standard deviation σ attained its minimum value; let this value be called σ_0. We then continue increasing the perturber mass until a $\sigma = 2\sigma_0$ is reached, which we still consider acceptable and which is represented in Figure 4 by the empty triangles. This gives a conservative estimate of the maximum permissible perturber mass. The right-hand panels show the result of applying the K-S test to the fits. The K-S indicator, Q, shows an excellent fit (large dots) to the full squares (corresponding to σ_0), and an acceptable fit (small dots) to the triangles (corresponding to $2\sigma_0$) for all but the largest semiaxes.

To further refine our results we tried an alternative method. Figure 5 shows the result of applying the K-S test to different observed samples, using two power-law fits for the unperturbed and perturbed regions, respectively. The figure shows an excellent agreement ($Q = 1$, as shown in the right-hand scale) for the entire observed range of semiaxes.

We now compare the cumulative distribution of semiaxes of the virtual binaries obtained from the dynamical model to these fits, using again the K-S test as criterion of goodness of fit and constructing the virtual binary samples as described above. Figure 6 illustrates the results we obtain for the 100, 50, and 25 most halo-like binaries. The full diamonds denote the observed samples, the crosses the best fits (which fix σ_0), and the empty triangles the still-permissible fits (corresponding to $2\sigma_0$). The goodness of these fits, as shown by the K-S indicator Q, is displayed in the right-hand scale of the panels. This method avoids binning the data, and thus allows a better resolution. Even for the comparison with the 100 most halo-like stars, the statistical errors of the modeled binaries remain negligible, since each virtual binary is constructed as the centroid of more than 500 evolved model binaries.

3. APPLICATION TO THE IMPROVED CATALOG OF CANDIDATE HALO BINARIES

As shown above for three samples, we are now ready to apply our dynamical model to different subsets of binaries extracted from our catalog (Allen & Monroy-Rodríguez 2014). For this study, we consider mainly the 150 binaries with computed galactic orbits. The galactocentric orbits were integrated using the standard Allen & Santillán (1991; axysimmetric) galactic
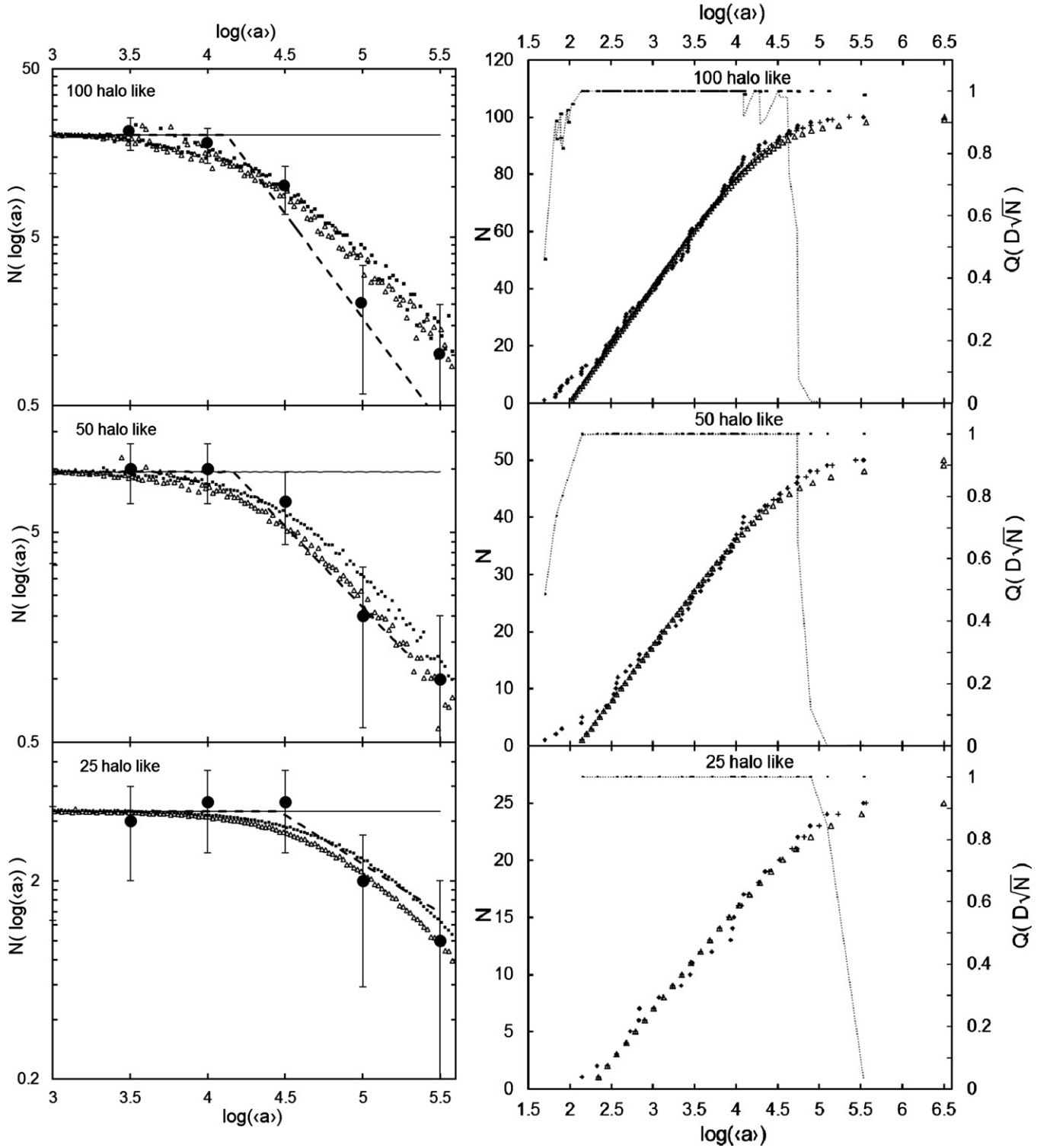
Figure 4. Fits of the evolved model distribution to different samples of binaries. The squares show the best fit, which defines σ_0 (see the text), and correspond to perturber masses of 16, 7, and 2 $M_\odot$ for the 100, 50, and 25 most halo-like stars, respectively. The triangles correspond to fits to $2\sigma_0$, which we still consider acceptable, and give more conservative estimates for the perturber mass: 21, 11, and 3 $M_\odot$ for the 100, 50, and 25 most halo-like stars, respectively. The right-hand panels display the results of applying the K-S test to these fits. The large dots correspond to the squares (σ_0) and show that the fit is excellent ($Q = 1$) for the entire range of semiaxes. The small dots correspond to the triangles ($2\sigma_0$) and show that the fit is still acceptable for all but the largest semiaxes.
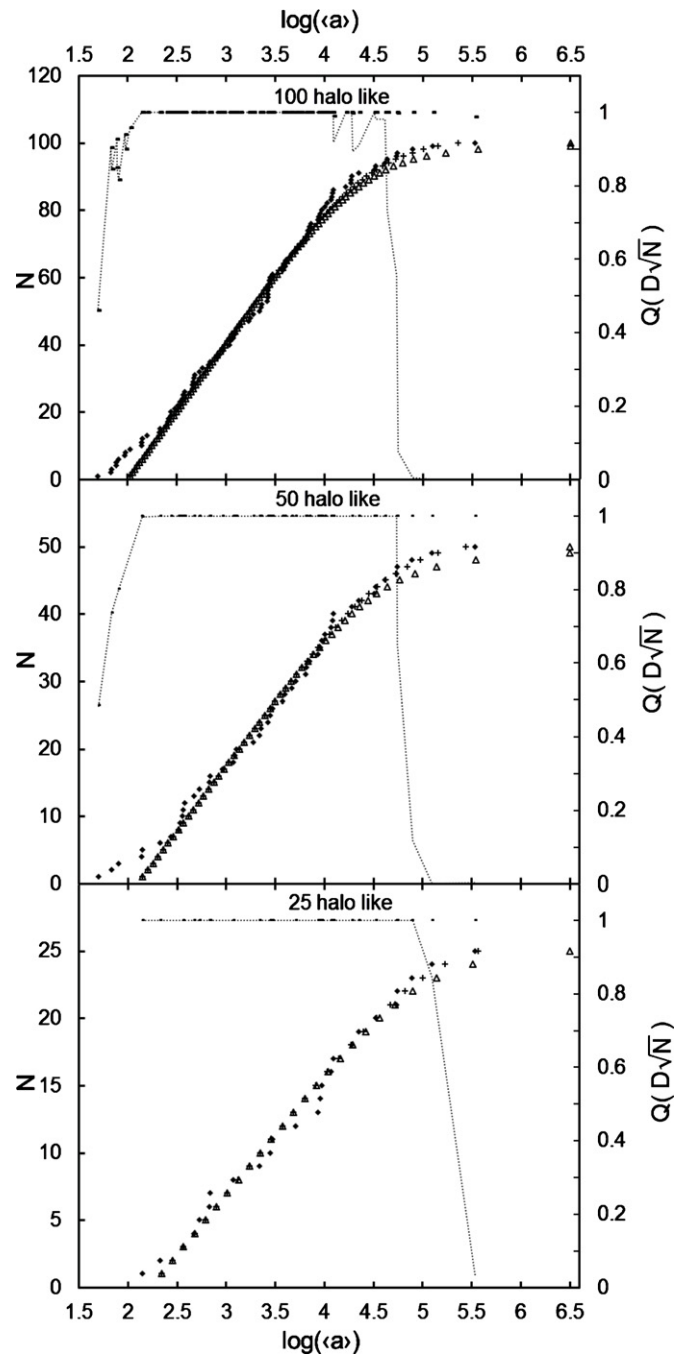
potential. Since very few orbits approach the zone of influence of the bar, an axisymmetric potential was found to be adequate. The orbits were integrated backward in time for 10 Gyr. The relative energy error amounted to less than 10^{-7} at the end of the integration. To establish membership to the halo, we calculate the time the binary spends within the galactic disk

($z = \pm 500$ pc). In Table 1, we display our main results. The different samples of binaries listed in Column 1 are ordered by the time they spend in the disk. Thus, the first entry corresponds to the 25 most halo-like binaries, which spend an average of only 0.08 of their lifetimes in the disk. The second column lists the fraction of their lifetimes the binaries spend in the disk.
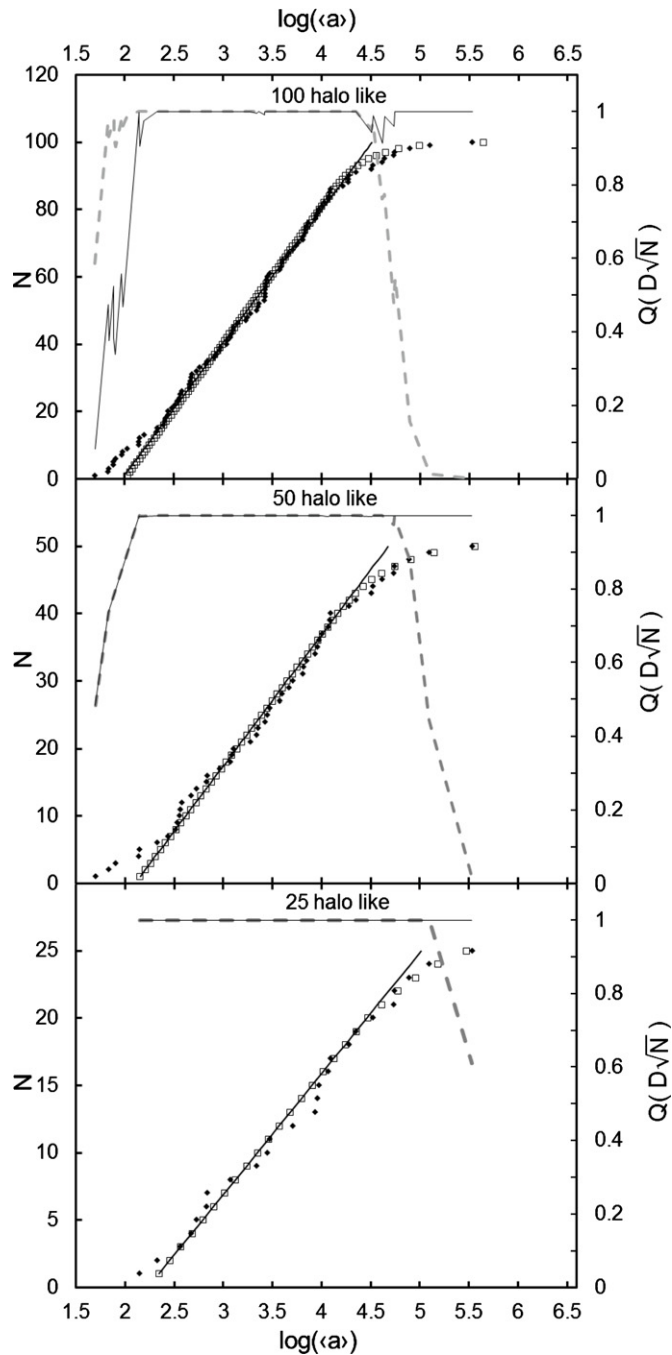
Figure 5. Cumulative distributions of observed semiaxes for three samples of binaries from our catalog, displayed by diamonds. The K-S test was applied to both a single Oepik-like fit (exponent 1) and to a two-power-law fit, with an Oepik-like distribution for the unevolved region and a steeper power law for the evolved region. The Q indicator for the single power-law fit, plotted on the right hand axis, shows an excellent fit for the unevolved region but drops after a certain value of the semiaxes (dashed lines). The two power-law fits are able to represent well the entire region, as shown by the empty squares and the Q indicator (full line).

Figure 6. K-S fits to the evolved binaries. The thin dotted horizontal line at $Q = 1$ (and the small dots extending it) is the Q indicator for the best fit (shown by crosses), which defines σ_0. The dropping dotted line is the Q indicator for the still acceptable fit to $2\sigma_0$, shown as triangles. The diamonds represent the observed samples. The $2\sigma_0$ fits by this method give maximum perturber masses of 21, 11, and 3 $M_\odot$ for the 100, 50, and 25 most halo-like stars, respectively.

Column 3 displays the upper limits obtained for the binned data for each group of binaries, with the fits performed to 2σ. Column 4 shows the limits obtained taking into account, on average, the variable halo density encountered by the binaries along their galactic trajectories. These two columns are labeled with the subscript "b", to denote that the results were obtained from the binned data. Column 5 shows the MACHO mass limits we obtain using our alternative fitting method (K-S) which avoids

binning the data. Column 6 lists the corresponding results for a variable halo density. We shall further discuss these entries in Sections 4 and 5. Columns 5 and 6 are labeled K-S to denote that results were obtained using the K-S method.

4. ESTIMATE OF THE DYNAMICAL EFFECT OF THE DISK

We still have to take into account the dynamical interactions that the binaries experience during their passage through the galactic disk. These effects have not been considered in previous
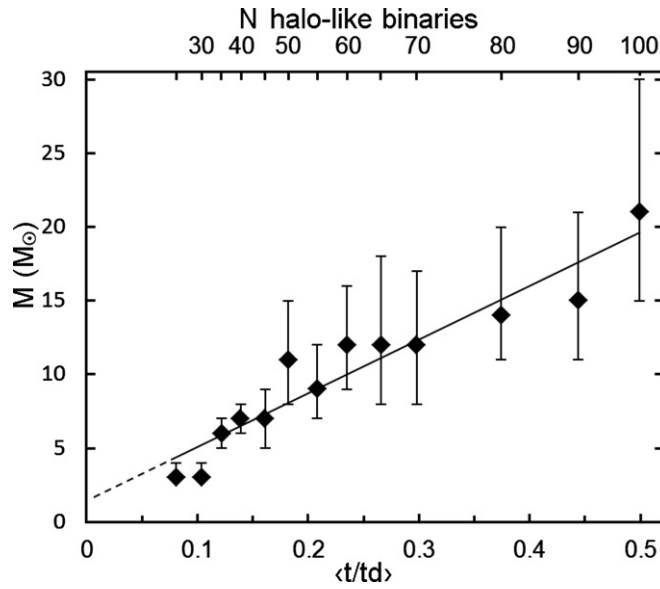
Figure 7. Maximum perturber masses for different groups of binaries from our catalog plotted against time spent within the disk. The error bars shown correspond to assumed distance errors of ±20%.

Table 1
Upper Limits for the Mass of the Massive Compact Halo Objects (MACHOs)

Sample[a]	$\langle T_d/T_t \rangle$	$M(\rho_0)_b$ $(M_\odot)$	$M(\langle \rho \rangle)_b$ $(M_\odot)$	$M(\rho_0)_{KS}$ $(M_\odot)$	$M(\langle \rho \rangle)_{KS}$ $(M_\odot)$
25	0.08	12	11	3	3
30	0.10	16	13	3	3
35	0.12	19	17	6	5
40	0.14	23	22	7	7
45	0.16	34	33	7	7
50	0.18	39	41	11	12
55	0.21	43	48	9	10
60	0.24	45	55	12	13
65	0.27	51	58	12	15
70	0.30	54	61	12	15
80	0.37	63	68	14	18
90	0.44	67	73	15	19
100	0.50	68	78	21	28
Yoo[b]		80		31	
Quinn[c]		105		32	

Notes.
[a] Number of most halo-like binaries with computed galactic orbits.
[b] 90 halo binaries of ChG.
[c] 89 halo binaries of Quinn et al. (2009).

studies (Yoo et al. 2004; Quinn et al. 2009). At this stage, we shall not attempt a full dynamical modeling but instead roughly estimate the effects of the disk passages by studying groups of binaries that spend progressively smaller fractions of their lifetimes within the disk. These fractions were obtained from the galactic orbits computed with the Allen & Santillán (1991) mass model. The result of this estimate is shown in Figure 7 where we display the MACHO masses obtained by applying the dynamical model to the groups of binaries listed in Table 1. The error bars in Figure 7 represent an estimate of the effect of the distance errors of the observed samples. Since we order our binaries by the time they spend within the disk, only average values of the distance uncertainties can be given for each group. These averages translate into average uncertainties in the expected major semiaxes. We re-computed the dynamical models to obtain best fits with probable errors of

Table 2
Effect of Distance Errors (20%) on Maximum MACHO Masses[a]

Sample[b]	+20%	0	−20%
25	3	3	4
30	3	3	4
35	5	6	7
40	6	7	8
45	5	7	9
50	8	11	15
55	7	9	12
60	9	12	16
65	8	12	18
70	8	12	17
80	11	14	20
90	11	15	21
100	15	21	30

Notes.
[a] For a constant halo density, adopting Couteau's formula.
[b] Number of most halo-like binaries with computed galactic orbits.

20% added to and subtracted from the expected semiaxes. We used these results to determine the error bars shown in Figure 7. On average, the maximum MACHO masses vary by about 20%, somewhat more than they do by adopting two alternative formulae for transforming the observed linear separations into expected major semiaxes. These results are displayed in Table 2. Taking the last point in the graph, we find a maximum MACHO mass of less than 5 $M_\odot$.

We remark that the smallest group, the 25 most halo-like binaries includes 6 very wide systems with concordant radial velocities, as reported in the literature. Therefore, their physical association can be considered to be established. Five of these binaries are among the widest known, and thus particularly suitable for determining upper limits to the masses of the perturbers. Since the 25 most halo-like binaries form a very interesting group for further studies (especially for determining the radial velocities of both components, and thus confirming—or not—their physical nature), we list them in Table 3, along with their main characteristics.

Columns 1 and 2 contain the designation of the primary and secondary components, respectively, while Column 3 lists our adopted distance. Columns 4 and 5 display the absolute visual magnitudes of the primary and secondary, respectively. Column 6 lists the projected separation in arcsec, and Column 7 the expected value of the major semiaxis in AU. Column 8 displays the peculiar velocity of the binary, and Columns 9, 10, and 11 the main characteristics of its galactocentric orbit, namely, the maximum distance from the galactic center, the maximum distance from the galactic plane, and the eccentricity, respectively. In the last column we list the fraction of its lifetime spent by the binary in the galactic disk, that is, within $z = \pm 500$ pc.

5. ESTIMATE OF THE EFFECT OF CONSIDERING A NON-UNIFORM HALO DENSITY

As was already pointed out by Quinn et al. (2009), the density of the halo cannot be assumed to be uniform. This is particularly relevant for galactic orbits that reach large apogalactic distances or large distances from the plane. To obtain a rough estimate of the effect of this non-uniform density on the computed mass

Table 3
The 25 Most Halo-like Wide Binaries

Primary	Secondary	d (pc)	M_V(p)	M_V(s)	s ($''$)	$\langle a \rangle$ (AU)	v_p (km s^{-1})	R_{max} (kpc)	$|z_{max}|$ (pc)	e	td/t
(1)	(2)	(3)	(4)	(5)	(6)	(7)	(8)	(9)	(10)	(11)	(12)
NLTT 16394[a]	NLTT 16407[a]	348	4.5	7.6	698.5	340309	481.5	144.0	88786	0.90	0.003
NLTT 37787	NLTT 37790	193	9.9	6.4	200.9	54283	470	115.2	109015	0.92	0.003
NLTT 4814	NLTT 4817	153	10.7	5.2	24.4	5139	303	12.9	8058	0.98	0.006
NLTT 5781	NLTT 5784	306	11.6	7.1	52.1	22320	380.4	44.2	32637	0.91	0.019
NLTT 18775	G090-036B	293	5.4	8.8	1.67	685	515.8	429.1	53116	0.96	0.020
NLTT 18346[a]	NLTT 18347[a]	167	5.1	4.3	11.9	2805	290.3	21.6	17469	0.52	0.028
NLTT 49562[a]	G 262-022r[a]	281	6.7	7.2	29.54	12155	370.5	40.0	27828	0.98	0.031
NLTT 1036	NLTT 1038	290	10.8	6.0	22.5	9135	213	9.8	7363	0.29	0.049
NLTT 32187	VBS 2	80	3.8	7.8	1.9	213	356.1	22.0	9995	0.94	0.055
NLTT 41756	VB 6	256	6.3	8.7	1.5	537	515.9	19.9	6958	0.43	0.060
NLTT 10536[a]	NLTT 10548[a]	214	4.6	9.1	185.7	55410	417.5	9.6	5202	0.12	0.062
NLTT 43097[a]	G 017-027j[a]	48	6.2	10.5	1170.7	79139	162.7	9.4	5692	0.69	0.074
NLTT 39442	LP 424-27	132	6.4	6.6	677	125073	306.7	15.6	7088	0.87	0.075
NLTT 5690	LP 88-69	71	4.1	9.1	22	2198	183.7	8.6	4562	0.51	0.083
NLTT 39456[a]	NLTT 39457[a]	29	6.7	7.1	300.7	12380	592.2	67.0	6410	0.86	0.088
NLTT 16062	BD 34 567	70	6.6	10.4	12	1176	265.5	11.8	6401	0.94	0.103
NLTT 9798	LP 470-9	100	3.6	7.6	1	140	104.5	8.7	2366	0.10	0.121
NLTT 52786	NLTT 52787	167	5.8	5.3	2	468	162.4	9.7	3623	0.58	0.123
NLTT 16629	NLTT 16631	55	6.4	10.5	434.1	33416	179.6	8.9	2562	0.29	0.125
NLTT 19979	NLTT 19980	344	7.9	10.2	19.6	9439	228.1	15.0	8120	0.92	0.135
NLTT 38195	BD+06 2932B	73	6.1	9.0	3.6	443	267.6	18.1	10301	0.96	0.137
NLTT 51780	G093-027B	136	6.0	8.7	3.52	672	259.8	14.4	2596	0.45	0.149
NLTT 525	NLTT 526	251	4.8	7.4	8.5	2986	361.3	31.6	3122	0.92	0.157
NLTT 14005	NLTT 13996	103	5.7	12.6	133	19173	101.9	8.7	2000	0.20	0.157
NLTT 17770	LP 359-227	180	4.1	10.4	34	8565	262.7	11.7	8661	0.96	0.158

Note. [a] Wide binaries with concordant radial velocities.

limits, we calculated for each binary a time-averaged halo density over its galactic orbit, using the halo mass distribution of Allen & Santillán (1991). Then, we averaged over the binaries in each studied group. The average densities turned out not to be very different from the density at the solar distance. This is due to the fact that, since the sample of binaries is restricted to nearby stars, orbits that reach large apogalactic distances also penetrate close to the galactic center, where they encounter large densities. Only a few binaries reaching large z-distances encounter considerably smaller average halo densities. As an aside, we point out that our orbit for NLTT 10536/10548 differs significantly from that plotted by Quinn et al. (2009). Our orbit reaches a z_{max} of only 5.2 kpc, instead of the almost 40 kpc in Quinn et al. This may partially account for the differences in the average halo densities we found, which are much less significant than those obtained by the former authors. The result of estimating the effects of a variable halo density is shown in Figure 8, for the groups of binaries in Table 1. The figure shows the mass limits obtained as a function of the fraction of time spent in the disk for each group for the average densities as described above and can be compared with Figure 7. The fits to obtain the limiting masses were performed using the unbinned data sets. From the last point in the graphs it is seen that the limiting masses obtained are less than 5 $M_\odot$. If we extrapolate to zero the time spent in the disk, we see that the maximum MACHO mass decreases to about 3 $M_\odot$.

If instead of using the Couteau (1960) formula for transforming observed separations into expected major semiaxes we use the expression derived by Bartkevičius (2008), we obtain the results shown in Table 4. The table shows that the derived limits increase somewhat, but this increase (on average about 5%) does not significantly alter the main conclusions of this study.
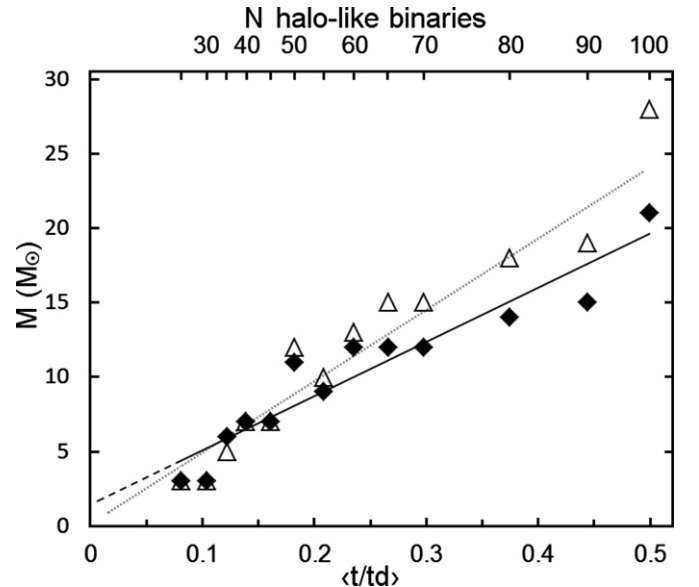
Figure 8. Maximum perturber masses for different groups of binaries plotted against time spent within the disk. The full diamonds correspond to a uniform halo density. The empty triangles show the effect of taking into account the variable halo density encountered on average by the different groups of binaries along their galactic trajectories.

Finally, Figure 9 shows the exclusion contours resulting from the present study and obtained using the prescription of Quinn et al. (2009). Our results, taken together with the microlensing data, practically exclude the presence of MACHOs in the galactic halo.
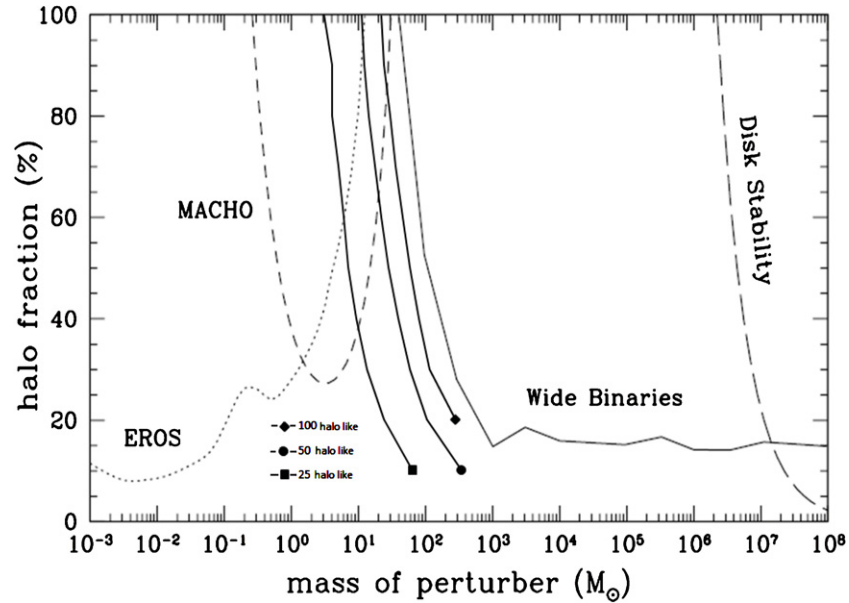
Figure 9. Exclusion contours for three different binary samples from our catalog. For comparison, we plot also the result of Yoo et al. (2004), labeled as "wide binaries." The contours plotted correspond to the results using unbinned data and the K-S criterion Q for goodness of fit (see also Table 1).

Table 4
Comparison of Upper Limits to the MACHO Masses
Using Two Estimates for $\langle a \rangle$, for a Constant Halo Density

Sample[a]	Couteau $M(\rho_0)$	Bartkevičius $M(\rho_0)$
25	3	4
30	3	4
35	6	6
40	7	8
45	7	8
50	11	12
55	9	9
60	12	13
65	12	14
70	12	14

Note. [a] Number of most halo-like binaries with computed galactic orbits.

6. SUMMARY AND CONCLUSIONS

From a catalog of 251 candidate halo wide binaries, we have extracted different subgroups in order to determine upper bounds to the MACHO masses. For a group of 150 binaries it was possible to compute galactic orbits and thus to evaluate the time they spend within the galactic disk. We developed and validated a dynamical model for the evolution of wide halo binaries subject to perturbations by MACHOs. This model was applied to different subsamples from the catalog, thus allowing us to obtain the following values as upper limits for the masses of MACHOs:

From 211 systems likely to be halo binaries: 112 $M_\odot$.

From 150 halo binaries with computed galactic orbits: 85 $M_\odot$.

From 100 binaries that spend the shortest times within the disk (on average, half their lifetimes): 21–68 $M_\odot$.

From the same 100 binaries, but taking into account the non-uniform halo density: 28–78 $M_\odot$.

From the 25 most halo-like binaries (those that spend on average 0.08 of their lifetimes within the disk): 3–12 $M_\odot$.

MACHOs have been strong candidates for the dark matter that appears to dominate the mass of galaxies, at least at large radii. Microlensing experiments (Tisserand et al. 2007, Wyrzykowski et al. 2009, 2011) exclude baryonic MACHOs with masses in the range 10^{-7} to 30 $M_\odot$ as dominant constituents of the dark matter halo. Other studies (Lacey & Ostriker 1985; De Rújula et al. 1992) have ruled out MACHO masses larger than about $10^6 \, M_\odot$. Wide binaries, as studied by Yoo et al., restricted the range of possible MACHO masses to 30–45 $M_\odot$, but their results were shown by Quinn et al. to critically depend on one of their widest binaries, which turned out to be spurious. Excluding this binary, Quinn et al. found a less stringent upper limit of about 500 $M_\odot$.

In the present study, we have used an expanded catalog of candidate halo wide binaries along with their galactic orbits to revise the limits for the MACHO masses. From different subsamples of binaries we obtain maximum MACHO masses ranging from 112 $M_\odot$ all the way down to less than 10 $M_\odot$. The most stringent limits are obtained from the most halo-like sample of 25 wide binaries, a sample particularly suited for further studies. These results, once again, all but exclude the existence of MACHOs in the galactic halo.

REFERENCES

Alfonso, C., Albert, J. N., Anderson, J., et al. 2003, A&A, 400, 951
Allen, C., & Monroy-Rodríguez, M. A. 2013, RMxAA(SC), 43, 13
Allen, C., & Monroy-Rodríguez, M. A. 2014, ApJ, in press
Allen, C., Poveda, A., & Hernández-Alcántara, A. 2007, in IAU Symp. 240, Binary Stars as Critical Tools and Tests in Contemporary Astrophysics, ed. W. I. Hartkopf, E. F. Guinan, & P. Harmanec (Cambridge: Cambridge Univ. Press), 405
Allen, C., Poveda, A., & Herrera, M. A. 2000, A&A, 356, 529
Allen, C., & Santillán, A. 1991, RMxAA, 22, 255

Bartkevičius, A. 2008, BaltA, 17, 209
Chanamé, J., & Gould, A. 2004, ApJ, 601, 289 (ChG)
Couteau, P. 1960, JO, 43, 41
De Rújula, A., Jetzer, P., & Massaó, E. 1992, A&A, 254, 99
Hartkopf, W. I., & Mason, B. D. 2007, Sixth Catalog of Orbits of Visual Binary Stars, WDS06 (Washington, DC: U. S. Naval Observatory)
Lacey, G. C., & Ostriker, J. P. 1985, ApJ, 299, 633
Lépine, S., & Bongiorno, B. 2007, AJ, 133, 889
Mason, B. D., Wycoff, G. L., Hartkopf, W. I., Douglass, G. G., & Worley, C. E. 2001, AJ, 122, 3466
Nissen, P. E., & Schuster, W. J. 1991, A&A, 252, 457
Poveda, A., & Allen, C. 2004, RMxAA(SC), 21, 49
Poveda, A., Allen, C., & Hernández-Alcántara, A. 2007, in IAU Symp. 240, Binary Stars as Critical Tools & Tests in Contemporary Astrophysics, ed. W. I. Hartkopjf, E. F. Guinan, & P. Harmanec (Cambridge: Cambridge Univ. Press), 417
Poveda, A., Allen, C., & Herrera, M. A. 1997, in Visual Double Stars: Formation, Dynamics and Evolutionary Tracks, ed. J. A. Docobo, A. Elipe, & H. McAlister (Astrophysics and Space Science Library, Vol. 223; Dordrecht: Kluwer), 191

Poveda, A., & Henández-Alcántara, A. 2003, in Sixth Pacific Rim Conference, Stellar Astrophysica, ed. K. S. Cheng, D. C. Leung, & T. S. Li (Astrophysics and Space Science Library, Vol. 298; Dordrecht: Kluwer), 111
Poveda, A., Herrera, M. A., Allen, C., Cordero, G., & Lavalley, C. 1994, RMxAA, 28, 43
Quinn, D. P., Wilkinson, M. I., Irwin, M. J., et al. 2009, MNRAS, 396, L11
Ryan, S. G. 1992, AJ, 104, 1144
Sesar, B., Ivezic, Z., & Juriic, M. 2008, AJ, 689, 1244
Tisserand, P., Le Guillou, L., Afonso, C., et al. 2007, A&A, 469, 387
Valtonen, M. 1997, in Visual Double Stars: Formation, Dynamics and Evolutionary Tracks, ed. J. A. Docobo, A. Elipe, & H. McAlister (Astrophysics and Space Science Library, Vol. 223, Dordrecht: Kluwer), 241
Widrow, L. M., Pym, B., & Dubinski, J. 2008, ApJ, 679, 1239
Wyrzykowski, L., Kozlowski, S., Skowron, J., et al. 2009, MNRAS, 397, 1228
Wyrzykowski, L., Skowron, J., Kozlowski, S., et al. 2011, MNRAS, 416, 2949
Yoo, J., Chanamé, J., & Gould, A. 2004, ApJ, 601, 311
Zapatero-Osorio, M. R., & Marttín, E. L. 2004, A&A , 419, 167